A Partial Proton Transfer in Hydrogen Bond O – H···O in Crystals of Anhydrous Potassium and Rubidium Complex Chloranilates

ARTICLE *in* THE JOURNAL OF PHYSICAL CHEMISTRY A · MARCH 2011

Impact Factor: 2.69 · DOI: 10.1021/jp112380f · Source: PubMed

THE JOURNAL OF PHYSICAL CHEMISTRY A

ARTICLE

pubs.acs.org/JPCA

A Partial Proton Transfer in Hydrogen Bond O—H···O in Crystals of Anhydrous Potassium and Rubidium Complex Chloranilates

Nikola Biliškov,[†] Biserka Kojić-Prodić,[*,†] Gregor Mali,[‡,§] Krešimir Molčanov,[†] and Jernej Stare[‡]

[†]Rudjer Bošković Institute, POB 180, HR-10002 Zagreb, Croatia

[‡]National Institute of Chemistry, Hajdrihova 19, 1001 Ljubljana, Slovenia

[§]EN-FIST Centre of Excellence, Dunajska c. 156, SI-1000 Ljubljana

Supporting Information

ABSTRACT: Hydrogen bonding and proton transfer in the solid state are studied on the crystals of isostructural anhydrous potassium and rubidium complex chloranilates by variable-temperature single crystal X-ray diffraction, solid state ^{1}H NMR and IR spectroscopies, and periodic DFT calculations of equilibrium geometries, proton potentials, and NMR chemical shifts. Their crystal structures reveal neutral molecules of chloranilic acid and its dianions connected into a chain by O—H···O hydrogen bond. A strong hydrogen bond with a large-amplitude movement of the proton with NMR shift of 13—17 ppm and a broad continuum in IR spectra between 1000 and 500 cm^{-1} were observed. Periodic DFT calculations suggest that proton transfer is energetically more favorable if it occurs within a single pair of chloranilate dianion and chloranilic acid molecule but not continuously along the chains of long periodicity. The calculated chemical shifts confirm the assumption that the weak resonance signals observed at lower magnetic fields pertain to the case when the proton migrates to the acceptor side of the hydrogen bond. The detected situation can be described by a partial proton transfer.

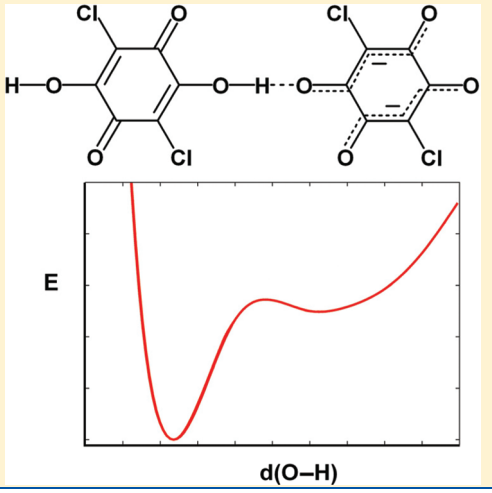

INTRODUCTION

The concept of hydrogen bonding was introduced about 90 years ago.[1−3] Geometric, spectroscopic, and thermodynamic parameters of the hydrogen bond are well-studied and described;[4−11] however, its dynamic aspects are just about to be understood.[12−23] Proton dynamics and, in particular, proton transfer processes are extremely fast, at a time scale of pico- and femtoseconds. Therefore, they can be directly studied only by the most advanced time-resolved spectroscopic methods (femtosecond laser UV/vis and IR/Raman).[21,22] Accurate high-level *ab initio* calculations are available for very small systems (involving a few atoms in vacuum).[22−25] The proton dynamics in the condensed phase involves a large number of molecules and can be simulated by computationally demanding QM/MM methods.[12,13,22,26−28] Additionally, a combination of *ab initio* calculations and IR spectroscopy can be used to study proton transfer in small molecular clusters in a vacuum.[29−31] Ultimately, DFT calculations in the crystalline state featuring periodic boundary conditions in conjunction with localized atomic or plane-wave basis sets are recently gaining importance, offering powerful support for the studies of the structure of solids.[32−34]

The study of proton transfer in the solid state is a rather complex task. Variable-temperature spectroscopy (IR/Raman and NMR)[35] and diffraction methods (X-ray and neutron)[36,37] can provide some indirect evidence of proton dynamics: temperature variation of equilibrium structure can be obtained. Crystallographic data can also be used as a starting point for periodic DFT calculations.[38−41] In a carefully designed experiment, hydrogen atoms can be located using X-ray diffraction; in the case of dynamic protons, a distribution of electron density in the hydrogen bond can be obtained.[36,37,42] The combinations of variable temperature X-ray and neutron diffraction are especially powerful, since these two methods are complementary, providing electron density distribution and the accurate position of the proton, respectively.[37,43−50]

In the case of proton transfer, one observes a broad continuum in IR spectrum. Occurrence of this feature is well established by Georg Zundel, and thus it is known as the Zundel continuum.[51−58] Shortly, these continua are often observed in systems with extensive intermolecular hydrogen bonding, for which equilibrium of the type A—H···B ⇌ A$^-$···H—B$^+$ is valuable. This continuum is caused by the symmetrical hydrogen bonds with a double minimum potential well in which a proton is distributed between the two hydrogen-bonded molecules by tunneling. Such hydrogen bonds are extremely polarizable.[54] Thus, observation of such a spectral feature is used as a strong experimental significance

Received: December 30, 2010
Revised: March 3, 2011
Published: March 23, 2011

Scheme 1. Dissociation of Chloranilic Acid (H_2CA) Generates Anions with Delocalized Electrons (HCA^- and CA^{2-}, Respectively)

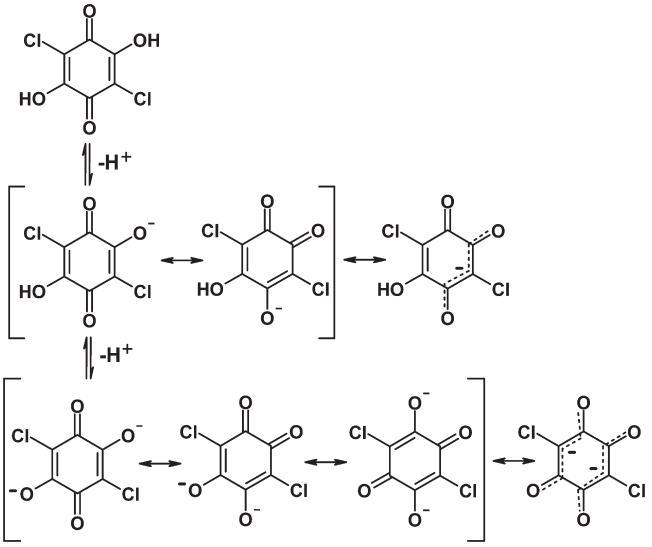

of the occurrence of proton transfer due to the strong hydrogen bonding of high symmetry regarding the distributed proton. The computational task is then to confirm it by establishing the separation of energy levels and the symmetry of the wave function.

Proton transfer dynamics study in the crystalline state is also a challenge for theorists. Recent examples, where dynamics studies have been complemented by X-ray and neutron diffraction studies, include the phosphoric acid−urea complex[41,59] and croconic acid, a promising organic ferroelectric material.[34] Our recent experience in this field features various techniques of molecular simulation, including *ab initio* molecular dynamics, vibrational analysis, and calculation of proton potential energy functions in systems containing short hydrogen bonds, such as tetraacetylethane[59] and sodium hydrogen bis-sulfate.[33]

A convenient system cannot be easily designed; therefore, the study of proton transfer in the solid state has been a great challenge. Crystals displaying temperature-dependent proton disorder in the ground state are few and in most cases have been obtained by serendipity, rather than by planned experiments. A proton location by X-rays becomes difficult (if not impossible) in large molecules or in the presence of heavy atoms due to the very low scattering power of the hydrogen atom. In some single crystal samples, proton transfer can be promoted by high pressure;[49,50,61,62] however, such systems are uncommon and X-ray measurement at high pressure is not always experimentally feasible.[63]

The proton transfer reactions are crucial in biocatalysis and other biological processes. These reactions are ultrafast, and very few experimental methods can be used to study proton dynamics. However, computer simulations can provide insight into the proton transfer reactions.[64−66]

The key issue of acid−base enzyme catalysis is proton transfer between two amino acid residues of an active site (for serine proteases from the catalytic Asp to His), and different theories on catalytic amino acid activities during catalytic cycles have been examined and tested by experimental and computational approaches over a few decades. Among them, the proposed transformation of a weak hydrogen bond in a free enzyme into a low-barrier hydrogen bond (LBHB) in the tetrahedral

Scheme 2. Hydrogen-Bonded Chains in Anhydrous Chloranilic Acid

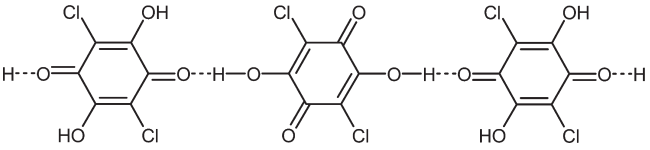

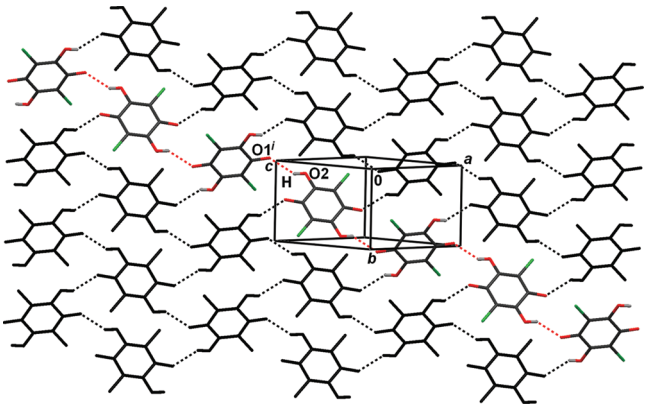

Figure 1. Layers parallel to (101) are generated by cross-linked hydrogen-bonded chains in the crystal structure of anhydrous chloranilic acid. Symmetry code used: (*i*) $-^1/_2 + x, {}^1/_2 - y, {}^1/_2 + z$.

intermediate during catalysis cycles of serine proteases was introduced in 1992 by Cleland[67] and further elaborated from 1994 to 2001.[68−73] The NMR studies and X-ray structure analysis of protein structures using data of high resolution [an ultrahigh resolution (0.78 Å) of subtilisin structure at pH 5.9[74]] performed on serine proteases over more than 30 years were analyzed and discussed and have became a subject of controversies on existence of LBHB and its possible role in biocatalysis.[75] Inconsistencies between theory and experiments cast doubt on the existence of LBHB within the enzyme active site.[76−79] However, possible formation of LBHB and its role in catalysis is not the only controversy in enzyme catalytic mechanisms. In biocatalysis, there are some other proposals, being a matter of long lasting discussions, such as "near attack conformations", enzyme dynamics during catalysis, quantum tunnelling, and entropic effects. Over the past decade, computational methods advanced significantly; chemical accuracy in QM/MM calculations[80] can predict barriers for enzyme-catalyzed reactions within 1 kcal mol^{-1} in the best cases.[81] Proton transfer dynamics in hydrogen bonds, involved in enzyme catalysis, is controlled by fluctuation of the polar environment, and proton tunneling can be correlated with protein dynamics.[82−84]

Dynamic proton disorder in the longest low-barrier hydrogen bond (2.74 Å) has been recently described in crystals of *p*-benzosemiquinone radical, an excited state of quinhydrone,[85] a cocrystal of unsubstituted benzoquinone and hydroquinone. Electronegative substituents on the quinoid ring stabilize the semiquinone radical, making the quinone an even stronger oxidant; they also influence its donor and acceptor potentials, facilitating proton disorder or proton transfer, accompanied by the formation of a low-barrier hydrogen bond. In a sophistically designed system, a proton transfer could occur in the ground state at room temperature and under atmospheric pressure.

A promising candidate for design of a solid-state proton-transfer system is anhydrous chloranilic acid, 2,5-dichloro-3,6-dihydroxy-1,4-benzoquinone ($H_2C_6Cl_2O_4$, H_2CA). It is a member of a broad class of 3,6-dihydroxy-benzoquinones with a general formula $H_2C_6X_2O_4$.[86−88] The electronic properties and structural characteristics of 1,4-benzoquionones are responsible for a variety of donor and acceptor functions that can be accompanied by a proton transfer and coupled with an electron transfer (Scheme 1).[89−92] We have extensively studied hydrogen bonding and proton transfer of chloranilic acid and its salts, and their multicomponent crystals.[85,93,94] The key issue is to predict and design a system capable of proton transfer.

Scheme 3. Hydrogen-Bonded Chains of $K_2[CA(H_2CA)]$ and $Rb_2[CA(H_2CA)]$ Comprise Alternating Molecules of Neutral Acid and Dianions with Delocalized Electrons

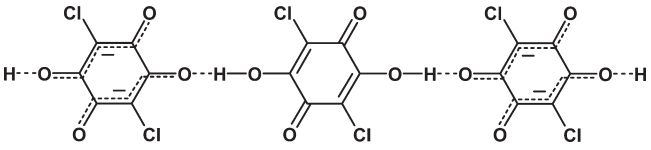

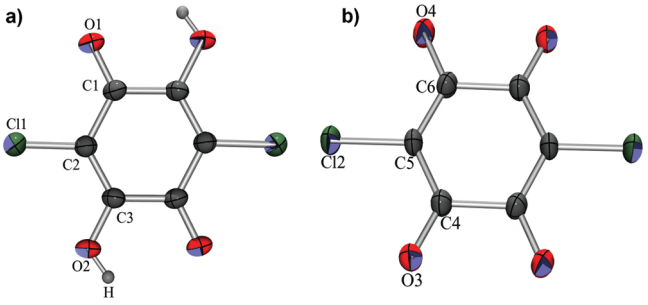

Figure 2. Molecular structures of C_i symmetry of (a) neutral chloranilic acid (with the inversion center located at $^1/_2$, $^1/_2$, $^1/_2$) and (b) chloranilate dianion (with the inversion center located at 0, 0, 0) in the crystal structure of $K_2[CA(H_2CA)]$ measured at RT. The atom numbering applies to all structures discussed. Displacement ellipsoids are drawn at the probability level of 50%, and the hydrogen atoms have been depicted as spheres of arbitrary radii.

The crystal structure of anhydrous chloranilic acid was originally determined from film data in 1967.[95] The structure comprises infinite hydrogen-bonded layers generated by two donors (OH groups) and two acceptors (carbonyl groups), Scheme 2, Figure 1; it can also be viewed as a network of quinhydrone-like cross-linked hydrogen-bonded chains.[96−98] Hydrogen chloranilate anion with a single proton is capable of forming a 1D chain, only (similar to those in Scheme 2). Such a system, being a strong donor and a very strong acceptor, could create strong hydrogen bonds involving proton and/or electron transfer in the solid state.[86−88] The proton transfer is facilitated by resonance, similarly as in *p*-benzosemiquinone.[85] Since both donor and acceptor originate from the same chemical species, they have close pK_a values, so the proton transfer is feasible, and semiquinone-like chains can be expected.

The anhydrous salts of potassium and rubidium hydrogen chloranilate are convenient systems to study the behavior of the proton in the less-common hydrogen bond. The analysis of the hydrogen bonds presented here is based on the variable temperature X-ray structure analysis, infrared spectroscopy, solid state ^{1}H NMR data, and periodic DFT calculations. The crystal structure of anhydrous chloranilic acid has been redetermined to obtain accurate geometric data for comparison.

RESULTS AND DISCUSSION

Crystal Structures of $K_2[CA(H_2CA)]$ and $Rb_2[CA(H_2CA)]$. According to the results of X-ray structure analysis, both salts, potassium and rubidium, are isomorphous at the level of non-hydrogen atoms. Surprisingly, the crystals do not comprise hydrogen chloranilate anions, but instead, hydrogen-bonded chains of alternating neutral chloranilic acid molecules and its dianions occur; both molecular species are of C_i molecular symmetry (Scheme 3, Figures 2 and 3, Table 1). The charge is balanced by two alkali cations, leading to the formation of salts $K_2[CA(H_2CA)]$ and $Rb_2[CA(H_2CA)]$. The values of bond distances of the dianion involving the atom sequence O3−C4−C5−C6−O4 and its centrosymmetric analogue reveal pronounced conjugation[99] (Scheme 1, Figure 2, and Table 1). The bond lengths of the carbonyl group and C−O^- are affected by conjugation [their difference is at the level of standard deviations, only: 1.248(3) Å in potassium compound; 1.242(5)

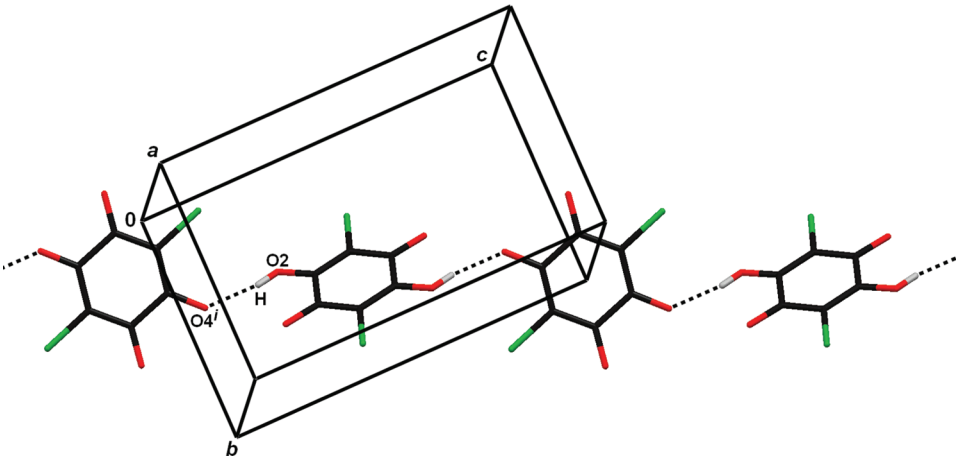

Figure 3. Hydrogen-bonded chains of alternating neutral chloranilic acid molecules and chloranilate dianions in the crystal structure of $K_2[CA(H_2CA)]$ extend in the direction [111]. Symmetry code: (i) $-1 + x$, $1 + y$, z.

dx.doi.org/10.1021/jp112380f |*J. Phys. Chem. A* 2011, 115, 3154–3166

Å in rubidium compound]. Each of two conjugated systems involves delocalized electrons (Scheme 3). The observed values are well-reproduced by the second-order Møller−Plesset (MP2) calculations reported by Ishida and Kashino for lutidinium salt of mono- and dianions of chloranilic acid.[100]

The neutral chloranilic acid molecule serves as a double donor, whereas its dianion acts as a double acceptor, generating an infinite hydrogen-bonded chain (Figure 3 and Table 2). According to geometric parameters (Table 2), these bonds can be characterized as strong hydrogen bonds.

The quality of room-temperature data of $K_2[CA(H_2CA)]$ allowed reliable location of the proton in a difference Fourier map (Figure 4): it reveals a single maximum located 0.8 Å from O2 and 1.7 Å from O4; its electron density is 0.5 e $Å^{-3}$. Such a maximum should indicate an ordered proton. For low- and high-temperature measurements, the position of the proton can be deduced from molecular geometries (heavy atom positions), which do not change significantly compared to the room-temperature structure. Unit cell parameters vary slightly with temperature in the range 100−340 K (Experimental Section), indicating no phase transition that could be expected in the case of proton disorder. A dynamically disordered proton would make both rings chemically equivalent (i.e., monoanion-like), which would result in a smaller unit cell. Due to the high electron density of the rubidium cation, the proton in $Rb_2[CA(H_2CA)]$ could not be accurately located, although hydrogen-bond geometries do not reveal significant differences compared to the potassium salt.

The crystal packing of both compounds was analyzed in detail to search for possible structural effects that originate from the different polarizability of K^+ and Rb^+. The alkali cations are octacoordinated (more details on cation coordination given in the Supporting Information), generating a double polymeric chain of polyhedra which are interconnected by hydrogen-bonded chains of chloranilic acid and its dianion into the three-dimensional network (Figure 5).

Spectroscopic Evidence of Partial Proton Transfer. Infrared and solid state ^1H NMR spectra of both compounds were recorded using single crystals (selected under stereomicroscope) to reveal the nature of the hydrogen bonds.

The groups OH and C═O are directly involved in intermolecular hydrogen bonding which causes considerable changes in corresponding vibrations, relative to the expected spectrum of the non-hydrogen-bonded species. Observed infrared spectra of solid H_2CA (for comparison), $K_2[CA(H_2CA)]$, and $Rb_2[CA-$

Table 1. Geometric Parameters of Molecules of Chloranilic Acid and Chloranilate Dianions[a]

	H_2CA	$Rb_2[CA(H_2CA)]$	$K_2[CA(H_2CA)]$
C1−C2	1.449 (2)	1.451 (6)	1.451 (4)
C2−C3	1.349 (2)	1.349 (6)	1.355 (3)
C3−C1	1.502 (2)	1.516 (6)	1.505 (3)
C1−O1	1.218 (2)	1.216 (5)	1.222 (3)
C3−O2	1.322 (2)	1.311 (5)	1.311 (3)
C2−Cl1	1.711 (2)	1.707 (5)	1.710 (3)
C4−C5		1.398 (6)	1.394 (3)
C5−C6		1.396 (6)	1.402 (3)
C6−C4		1.550 (6)	1.543 (3)
C4−O3		1.242 (5)	1.250 (3)
C6−O4		1.243 (5)	1.246 (3)
C5−Cl2		1.743 (4)	1.741 (2)

[a] CA = $(C_6Cl_2O_4)^{2-}$. Room temperature data are listed.

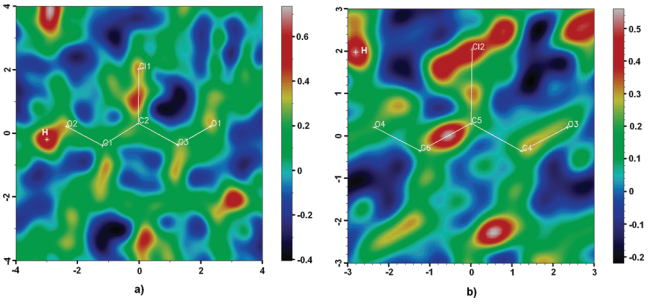

Figure 4. Difference Fourier maps for the structure of $K_2[CA(H_2CA)]$ at room temperature: (a) environment of the atom O2, (b) environment of the atom O4. The single maximum of 0.5 e $Å^{-3}$ near the atom O2 corresponds to a localized proton; its distance from O2 (donor atom) is 0.8 Å, and its distance from O4 (acceptor) is 1.7 Å.

Table 2. Measured and Calculated Geometric Parameters of Hydrogen Bonds[a]

	H_2CA	$Rb_2[CA(H_2CA)]$	$K_2[CA(H_2CA)]$ (100 K)	$K_2[CA(H_2CA)]$ (293 K)	$K_2[CA(H_2CA)]$ (calculated)[b]	$K_2[CA(H_2CA)]$ (320 K)
d(O2−H)/Å	0.80 (3)	0.83 (3)	0.82 (3)	0.81 (3)	1.035	0.82 (8)
d(H···O[c])/Å	2.08 (3)	1.84 (3)	1.80 (2)	1.85 (2)	1.596	1.85 (7)
d(O2···O[c])/Å	2.781 (2)	2.642 (5)	2.613 (2)	2.637 (3)	2.610	2.645 (8)
(O2−H···O[c])/Å	146 (3)	167 (7)	170 (5)	164 (4)	165	161 (2)
symm. op. on acceptor	$-^1/_2 + x, ^1/_2 - y, ^1/_2 + z$	$-1 + x, 1 + y, z$	$-1 + x, 1 + y, z$	$-1 + x, 1 + y, z$	$-1 + x, 1 + y, z$	$-1 + x, 1 + y, z$
d(H···O1)/Å	2.24 (3)	2.31 (6)	2.37 (5)	2.31 (4)	2.337	2.4 (2)
d(O2···O1)/Å	2.665 (2)	2.687 (5)	2.704 (2)	2.695 (3)	2.731	2.697 (8)
(O2−H···O1)/Å	113 (3)	108 (4)	105 (3)	110 (3)	101	103 (10)
symm. op. on acceptor	x, y, z	x, y, z	x, y, z	x, y, z	x, y, z	x, y, z

[a] CA = $(C_6Cl_2O_4)^{2-}$. [b] Single unit cell model. Values obtained from double and triple supercells differ from these values only marginally, the differences being of the order of a few thousandths of an Å (see Table 4). [c] Acceptor atoms: O1 for H_2CA and O4 for $Rb_2[CA(H_2CA)]$ and $K_2[CA(H_2CA)]$.

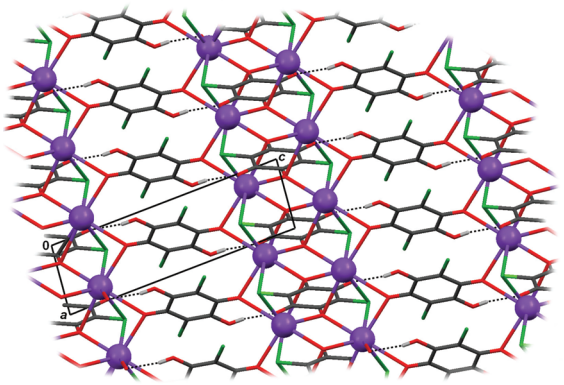

Figure 5. The crystal packing of isostructural $K_2[CA(H_2CA)]$ and $Rb_2[CA(H_2CA)]$ compounds. Double chains of edge-sharing polyhedra run in the direction [100]. The alkali ions (violet spheres) are arbitrarily scaled.

$(H_2CA)]$ are presented in Figure 6. The positions of the observed bands and their comparison with the spectrum of solid 2,5-dihydroxy-1,4-benzoquinone (DHBQ)[101] are given in Table 3. To obtain more reliable insight into the effect of hydrogen bonding and proton transfer, the spectra were compared with gas-phase (no hydrogen bonding) spectra of 1,4-hydroquinone (HQ)[102] and 1,4-benzoquinone (BQ).[103]

Stretching of the OH groups of H_2CA is represented by a rather asymmetric band, with a very broad shoulder at its low-wavenumber side. This asymmetry is interpreted as anharmonic coupling of high frequency with strongly damped low-frequency modes, reflecting medium-strong O−H···O hydrogen bonding. The ν(OH) band of HQ in the gas phase is located at 3662 cm^{-1},[102] while the corresponding band for gas-phase DHBQ is found at 3371 cm^{-1}.[101] The red shift of 291 cm^{-1} is interpreted by intramolecular O−H···O hydrogen bonding. The observed position of the ν(OH) band for solid H_2CA is interpreted analogously. In the case of solid H_2CA, the red shift of ν(OH) of 437 cm^{-1}, relative to the gas-phase HQ spectrum,[102] together with the overall shape of the absorption indicate intermolecular O−H···O hydrogen bonding, which is stronger than intramolecular hydrogen bonding in DHBQ.

As indicated in the footnotes of Table 3, Pawlukojć assigned the absorption at 1628 cm^{-1} for H_2CA to ν(C═C), while that at 1664 cm^{-1} to ν(C═O).[104] However, from the behavior of the corresponding spectral envelope, as observed for the spectra of DHBQ in the gas phase, solid phase, and chloroform solution, a more reliable interpretation is given by Szabó and Kovács.[101] The comparison of the spectral region 1700−1580 cm^{-1} for $K_2[CA(H_2CA)]$ and $Rb_2[CA(H_2CA)]$ with that of H_2CA (see Table 3) reveals that mainly the band at 1628 cm^{-1} (H_2CA spectrum) is changed, while that at 1664 cm^{-1} remains relatively unaffected. Accordingly, here we accept the interpretation given by Szabó and Kovács.[101] The observed red shift of the ν(C═O) band of H_2CA, relative to gas-phase BQ,[103] is 52 cm^{-1} corresponding to the moderately strong hydrogen bonding in H_2CA. This finding is supported by the d(O2···O) distance obtained from X-ray structure analysis (Table 2). The IR spectrum of 2,5-dihydroxy-1,4-benzoquinone shows the ν(OH) band at 3290 cm^{-1}, and ν(C═O) at 1630 cm^{-1},[101] indicating somewhat weaker hydrogen bonding than in H_2CA. The spectral data are in accordance with distances between donor and acceptor oxygen atoms, obtained by X-ray structure analysis (Table 2).

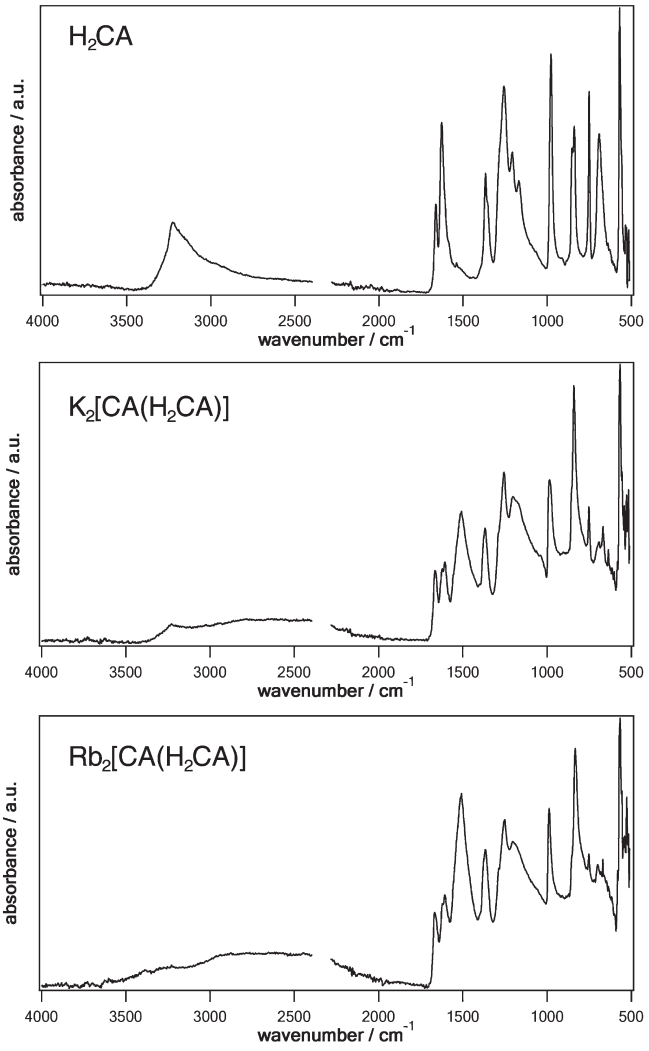

Figure 6. Infrared spectra of anhydrous chloranilic acid (top), $K_2[CA(H_2CA)]$ (middle), and $Rb_2[CA(H_2CA)]$ (bottom). The 2400−2280 cm^{-1} region is removed from the spectra due to the absorption of atmospheric CO_2. Occurrence of the bands at 1622 and 1607 cm^{-1} in the spectra of $K_2[CA(H_2CA)]$ and $Rb_2[CA(H_2CA)]$ and the band at 3228 cm^{-1} in the spectrum of $K_2[CA(H_2CA)]$ is assigned to contamination by H_2CA in the sample.

In the spectra of $K_2[CA(H_2CA)]$ and $Rb_2[CA(H_2CA)]$, characteristics typical of strong hydrogen bonding are detected (Figure 6). A band originating from the free or intramolecularly hydrogen-bonding ν(OH) completely disappears, giving rise to a very broad absorption in the 3500−2000 cm^{-1} range. This absorption at ∼2600 cm^{-1} is assigned to stretching vibration of a strongly hydrogen-bonded OH group. The red shift of the maximum position relative to the gas-phase 1,4-hydroquinone[102] is ∼1660 cm^{-1}, which is consistent with the observed d(O2···O*) intermolecular distance in $K_2[CA(H_2CA)]$ and $Rb_2[CA(H_2CA)]$ (Table 2), as expected by the Novak−Mikenda relationship.[105] The anharmonic coupling of the fast OH stretching motion with low-frequency modes of the O−H···O hydrogen-bonded system also contributes to the shift toward the lower wavenumbers, as well as to considerable band broadening. Additional evidence of the involvement of OH groups in the formation of the strong hydrogen bonds is the

Table 3. Characteristic Infrared Bands (Wavenumbers in cm^{-1}) in the 4000−500 cm^{-1} Range of 2,5-Dihydroxy-1,4-benzoquinone (DHBQ), H_2CA, $K_2[CA(H_2CA)]$, and $Rb_2[CA(H_2CA)]$

DHBQ[a]	H_2CA	$K_2[CA(H_2CA)]$	$Rb_2[CA(H_2CA)]$	assignment[b]
3371 s[c]				ν(OH)
3290 w	3225 m	2600 m, b	2600 m, b	ν(OH)
3096 w				ν(CH)
3094 w				ν(CH)
1671 s	1664 s	1664 s	1665 s	ν(C═C)[d]
1630 s	1628 s	1622 m	1623 m	ν(C═O)[d]
		1607 m	1607 m	ν(C═O)[e]
		1509 s	1511 s	hydrogen-bonded ν(C═O)[e]
1398 m	1367 s	1368 s	1367 s	ν(C—O)
	1354 m			
1256 w	1257 m	1255 s	1253 s	δ(COH)
	1208 m	1203 m	1204 m	δ(COH)
1172 w	1167 w	1170 w		δ(CCH)[a]
1124 m				δ(COH)[a]
1114 m				δ(COH)[a]
	978 s	986 m	988 s	ν(C—C)
	852 m	856 m	853 m	ν(C—Cl)
	840 m	840 m	834 m	ν(C—Cl)
750 w	750 m	752 w	752 w	C═O wagging
687 m	691 m	690 w	700 w	τ(CCOH)
668 w		668 w	669 w	δ(CC═O)
	569 s	567 s	567 s	C—Cl wagging[b]
505 m	503 m			ring deformation[a]

[a] Solid phase.[69] [b] Assignation according to ref 70. [c] From the gas-phase spectrum. [d] In ref 70, the 1664 cm^{-1} band is assigned to ν(C═O), while 1628 cm^{-1} to ν(C═O). However, much more reliable interpretation of these bands is given in ref 69. [e] Assignation as proposed in this work.

behavior of the torsional vibration of the OH group of H_2CA (Table 3).[104] This band disappears from the spectral range in the structure of $K_2[CA(H_2CA)]$ and $Rb_2[CA(H_2CA)]$. Obviously, this torsion is considerably damped by hydrogen-bond formation. Simultaneously, the intensity of the band due to ν(C═O) considerably decreases, while a very strong and broad band appears at 1510 cm^{-1}. Such a large red shift of the ν(C═O) band (169 cm^{-1} relative to the position of the corresponding band for gas-phase 1,4-benzoquinone[103]) and change of the band shape obviously reflect the effect of the same very strong hydrogen bonding to carbonyl groups of chloranilate anions in the crystals under consideration. Broadening of the band is attributed to the rather strong coupling of C═O and OH stretching vibrational motions due to the hydrogen bonding.

The continuum absorption spreading from 1500 cm^{-1} into the far-infrared region is a spectroscopic feature typical of the systems with strong hydrogen bonding associated with a considerable proton transfer.[51,106−108] This continuum is qualitatively similar to the Zundel continuum, i.e., spectral changes that occur in the spectra of H_2O upon the addition of strong acids or bases. Accordingly, the observed continuum is attributed to protons shared between two oxygen atoms of the neighboring OH and C═O groups, whose stretching potentials are rapidly modulated by fluctuations of the local environment in the $K_2[CA(H_2CA)]$ and $Rb_2[CA(H_2CA)]$ crystal. The continuum originates from the anharmonic double minimum potentials, allowing large amplitude proton motions and the high polarizability of such hydrogen bonds.[51] The proton transfer broadens the OH stretching potential, giving rise to a continuum of rapidly evolving structures with different proton potentials. The two wells on either side of the potential correspond to a proton covalently bonded to a different oxygen atom of a C—O—H···O═C intermolecular pair. However, the potential in this case is asymmetric, confining the proton transfer to only a certain amount, shifting the proton transfer equilibrium toward the left side. This asymmetric model of hydrogen bonding is consistent with observation of a significantly red-shifted, very broad ν(OH) band in the 3500−2000 cm^{-1} region, together with a considerably broadened and red-shifted ν(C═O) absorption peaking at 1508 cm^{-1}. The intensive continuum in the 1500−500 cm^{-1} region indicates relatively long-living species, which is consistent to the proposed two-well low-barrier model of hydrogen bonding in $K_2[CA(H_2CA)]$ and $Rb_2[CA(H_2CA)]$ (*vide infra*).

The intensity ratio of this band for $K_2[CA(H_2CA)]$ and $Rb_2[CA(H_2CA)]$ relative to the chloranilic acid is obtained by fitting this spectral region to three Lorentzian profile functions, centered at 1622, 1607, and 1508 cm^{-1}, respectively. The obtained intensity for the 1508 cm^{-1} band is normalized assuming constant intensity of the ν(C═C) band at 1661 cm^{-1}. According to the intensity ratio of ν(C═O), proton transfer is much more pronounced in $K_2[CA(H_2CA)]$ and $Rb_2[CA(H_2CA)]$ than in the pure acid. However, due to the limitations of the measuring method (see the Experimental Section), the results are not quantitative.

A reliable quantitative characterization of the observed continuum is not possible owing to numerous superimposed peaks in this region (Table 3, Figure 6), and the center of gravity of a continuum region cannot be determined reliably.

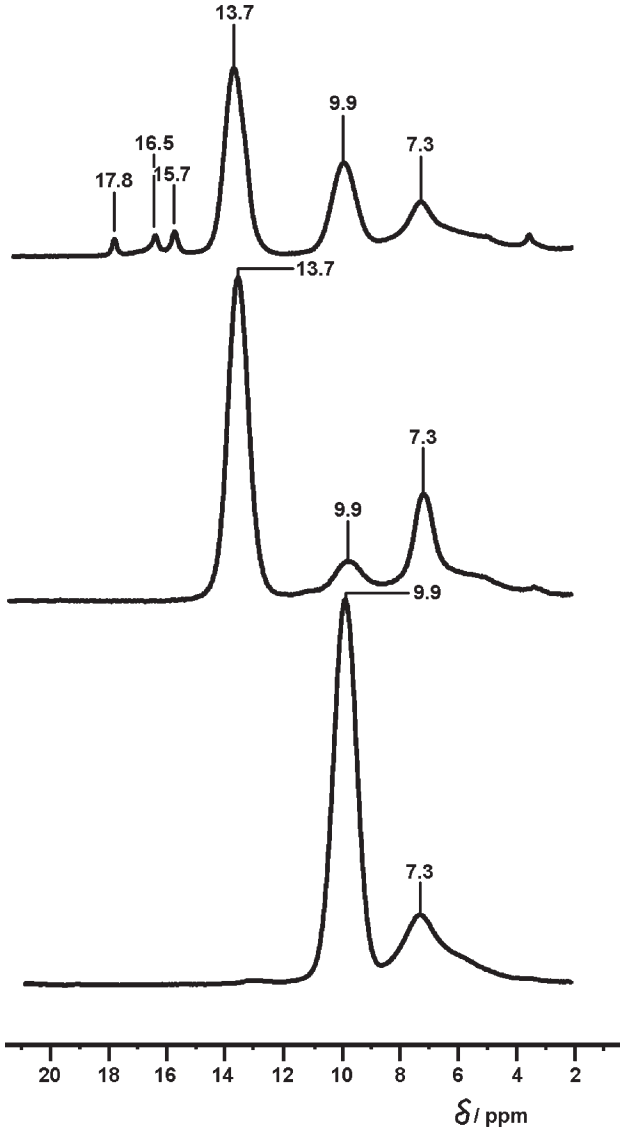

Figure 7. Solid state ^{1}H NMR spectra of anhydrous chloranilic acid (bottom), $Rb_2[CA(H_2CA)]$ (middle), and $K_2[CA(H_2CA)]$ compounds (top). The broad peak centered at 7.3 ppm is a result of aromatic impurities.

The interpretation of the solid state ^{1}H NMR spectra (Figure 7) was not straightforward due to inhomogenous samples. All samples showed a signal of the proton from chloranilic acid (9.9 ppm) (samples for measurements were selected under stereomicroscope and small amounts of free acid and reaction components or byproducts hardly can be avoided). A very broad signal around 7.3 ppm originates from impurities. The NMR spectrum of a DMSO solution of chloranilic acid revealed three weak signals with chemical shifts of 7.0, 7.2, and 7.4 ppm which belong to the aromatic and phenolic hydrogen atoms. The total amount of impurities is 4−8%. The proton signal in $Rb_2[CA(H_2CA)]$ at 13.7 ppm is intensive, whereas, in $K_2[CA(H_2CA)]$, it is weaker, and also located at 13.7 ppm. The potassium compound also revealed three weak, even more shifted signals at 15.7, 16.5, and 17.8 ppm. The signal with the largest shift may belong to a dynamically disordered proton and this assignment agrees with IR spectra (Figure 6). However, three signals of a single proton cannot be easily explained; one of the possible explanations could be the existence of three discrete states of the proton, which cannot be observed by X-ray analysis due to a low population and low scattering power of the hydrogen atom.

^{1}H NMR chemical shifts of $K_2[CA(H_2CA)]$, calculated for the global minimum structure (no proton transfer) and for various equilibrium structures with proton transfer, modeled in the unit cells of different size, are discussed in the following section.

DFT Calculations. Regardless of the model, full geometry optimization of $K_2[CA(H_2CA)]$ yields reasonable agreement with the diffraction-determined structure, justifying the choice of the applied methodology for the present study. Specifically, the hydrogen-bond geometry parameters listed in Table 4 are well matched with the experimental values. Exceptions to this are the interatomic distances involving hydrogen, since experimental assignments of the proton position with X-rays are known to notably underestimate the O2−H bond distance.[109,110] The calculated O2−H distance of 1.035 Å is probably more realistic than the diffraction-determined value of just over 0.8 Å (or the average O−H bond length of 0.82 Å[109,110]).

Attempts to identify another regular minimum energy structure with the proton nearer to O4 than to O2 (proton transfer within the $H_2CA\cdots CA^{2-}$ pair, yielding $HCA^-\cdots HCA^-$) were successful for all the unit cell models. The common feature of all the optimized proton transfer structures is that the so obtained hydrogen bond is significantly shorter (2.477−2.539 Å) than in the optimized $H_2CA\cdots CA^{2-}$ pair (2.607−2.610 Å). However, notable differences in the structure were observed for different sizes of the unit cell (Table 4). With a single $H_2CA\cdots CA^{2-}$ pair in the model (single cell), the proton transfer eventually affects all the chloranilate units in the crystal structure (eventually, with a single unit cell model, the KHCA compound is formed by the proton transfer), resulting in a strong cooperative effect within the infinite ...$HCA^-\cdots HCA^-$... chains and quite a dramatic shrinking of the O2···O4 distance. If the model unit cell is enlarged along the ...$H_2CA\cdots CA^{2-}$... network (double and triple "cell model"), it is possible to model proton transfer as a more "localized" process, in the sense that the replica $HCA^-\cdots HCA^-$ units obtained from proton transfer are separated by one or two "intact" $H_2CA\cdots CA^{2-}$ units, respectively, thus reducing the cooperative effect between the correlated neighboring cells. Thus, the resulting proton transfer structures differ less radically, yet still significantly, from their nontransferred counterparts.

The considerable shortening of the hydrogen bond on proton transfer should be reflected on the spectroscopic properties of the $HCA^-\cdots HCA^-$ moiety and should be different from ones in the $H_2CA\cdots CA^{2-}$ pair. Specifically, as can be concluded on the basis of established correlations between the donor−acceptor distance and spectroscopic observables,[111,112] the proton stretching mode is expected to be red-shifted and broadened, while the ^{1}H NMR chemical shift of the proton should be increased. Indeed, simple harmonic calculation of vibrational modes (single unit cell model) yields the OH stretching frequency of 2699 cm^{-1} for the $H_2CA\cdots CA^{2-}$ moiety, while by proton transfer the frequency is shifted to 1786 cm^{-1}. It should be noted that the harmonic approximation is probably not sufficient to faithfully reproduce the real spectral quantities and is thus not suitable for quantitative assignment of bands, but this calculation clearly demonstrates the large impact of proton transfer on the vibrational spectra of the corresponding structural entities.

Table 4. Selected Geometry Parameters and Relative Energies of $K_2[CA(H_2CA)]$, Calculated by Different Unit Cell Models and with the Proton Located at Either Side of the Hydrogen Bond

	$[H_2CA\cdots CA^{2-}]$ (no proton transfer) [distances in Å, energies in kcal/mol]				$HCA^-\cdots HCA^-$ (proton transfer) [distances in Å, energies in kcal/mol]			
model	d(O2···O4)	d(O2−H)	d(H···O4)	E	d(O2···O4)	d(O4−H)	d(H···O2)	E
single cell	2.610	1.035	1.596	0.00	2.477	1.112	1.380	3.27
double cell	2.609	1.035	1.597	0.00	2.493	1.084	1.425	2.47
triple cell	2.607	1.037	1.588	0.00	2.539	1.022	1.528	1.50

Table 5. ^{1}H NMR Chemical Shifts of $K_2[CA(H_2CA)]$, Calculated for the Global Minimum Structure (No Proton Transfer) and for Various Equilibrium Structures with Proton Transfer, Differing in the Size of the Unit Cell

model	δ_H (ppm)
single cell, no proton transfer	12.43
single cell, proton transfer	15.57
double cell, proton transfer	14.94
triple cell, proton transfer	13.11

Table 5 lists the ^{1}H NMR chemical shift values calculated for the representative cases when the proton resides at either side of the hydrogen bond. It can be clearly seen that the structure without proton transfer, which is energetically most favorable, yields a notably lower value of chemical shifts than the three distinct proton transfer structures. In the latter, the chemical shift is larger by 0.7−3.1 ppm and it seems to reasonably correlate with the O···O distance (Table 4). The agreement with the experimental assignment of resonance signals (observed at 13.7, 15.7, 16.5, and 17.8 ppm, Figure 7) is fairly good, particularly the relative increase of chemical shift upon proton transfer, confirming the assumption that small amounts of proton transfer structures exist in the system. Nevertheless, the present NMR computational study does not allow us to devise a more precise model for the structures that contribute to the observed weak resonance signals at low magnetic fields. Among the factors that limit the accuracy of our calculations are (i) symmetry issues—the *P*1 symmetry was assumed for all proton transfer models, rendering all the protons in the unit cell formally nonequivalent; (ii) size-consistency issues—although fairly large supercells were used for the calculation of chemical shifts, even larger models would be needed for their convergence to ∼0.1 ppm precision; regretfully, calculations using such large cells are prohibitively expensive; (iii) complete neglect of the quantum nature of the proton—nuclear quantum effects can contribute significantly to the calculated chemical shift values.[112,113]

All the observed proton transfer structures are energetically less favorable than their nontransferred counterparts, but the relative energy depends on the size of the unit cell. With a single cell model, the energy uptake requested for proton transfer is calculated to be 3.27 kcal/mol. When confining the proton transfer event by using an enlarged unit cell model, this value drops to 2.47 kcal/mol (double cell) and to 1.50 kcal/mol (triple cell), indicating that the proton transfer is notably more favorable when it occurs as an isolated event rather than continuously over the entire crystal structure. This view is also supported by the calculated proton potential functions (Figure 8). Apparently, the proton transfer structure in the single unit cell model corresponding to conversion of all the $H_2CA\cdots CA^{2-}$ pairs into $HCA^-\cdots HCA^-$ barely represents a regular minimum on the potential energy surface. When the proton transfer becomes more isolated, the corresponding minimum becomes more pronounced and the barrier is also lowered, supporting the view that the proton transfer is more likely to occur as an isolated event.

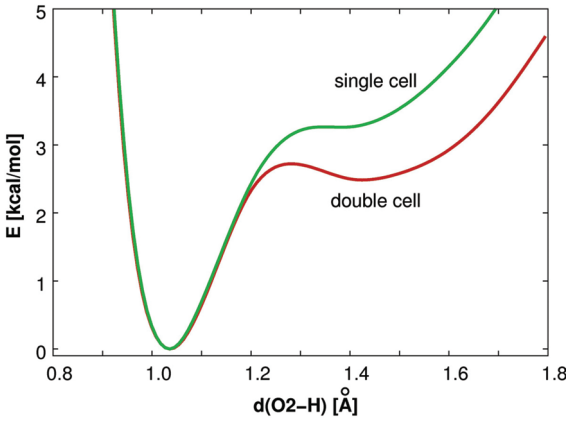

Figure 8. DFT potential energy function for proton transfer in the hydrogen bond of $K_2[CA(H_2CA)]$, calculated for the single and double unit cell model.

Given that the calculated energy differences between the global minimum and proton transfer structure are of the order of 3−5 k_BT at best, the abundance of the latter should be low even at room temperature. Indeed, in the tentative molecular dynamics run, structures with the proton closer to O4 than to O2 contributed only to a few percent of the entire population, which is in qualitative agreement with the experimental observations reported in this study. The fact that the proton transfer barrier is at least about 2 kcal/mol, requires sufficiently long simulation times in order to get satisfactory statistics on proton transfer dynamics. However, large unit cell models which would faithfully reproduce the isolated proton transfer process, coupled with tens of picoseconds of a simulation time, are at present prohibitively expensive. Instead, qualitatively well-supported evidence of proton transfer was reached.

CONCLUSION

Proton dynamics in the hydrogen bond O−H···O in crystals of anhydrous potassium and rubidium complex chloranilates was studied by X-ray structure analysis, IR and solid state ^{1}H NMR spectroscopies, and DFT calculations. X-ray structure analysis of the two isostructural compounds, $K_2[CA(H_2CA)]$ and $Rb_2[CA(H_2CA)]$, reveals hydrogen-bonded chains of neutral molecules of chloranilic acid and its dianion involving delocalized electrons. The strong hydrogen bond characterized by the short distance O···O of 2.613(2) Å in $K_2[CA(H_2CA)]$ (at 100 K) suggests a

partial proton transfer. The solid state NMR of $K_2[CA(H_2CA)]$ reveals three signals of a single proton that might be explained by existence of the three discrete states of the proton which cannot be observed in difference Fourier maps due to a low population and low scattering power of hydrogen atoms.

DFT solid state calculations show that the proton transfer is energetically more favorable when it occurs as an isolated event rather than continuously over the entire hydrogen-bonded chain in the crystal structure. The calculated ^{1}H NMR chemical shifts on structures with the proton located at either side of the hydrogen bond suggest that the resonance signals observed at low magnetic fields indeed correspond to the case where the proton resides at the acceptor site of the hydrogen bond; the relative energies of such structures are in agreement with the low integral intensity of these signals. Due to the complexity of the problem, a precise structural characterization of the proton transfer entities is beyond the reach of the present methodology. A pronounced continuum in the IR spectrum occurring in the 1500−500 cm^{-1} region is consistent with a two-well barrier model of hydrogen bonding involving a highly polarized proton, which is partially distributed between the two oxygen atoms involved in hydrogen bonding, through the equilibrium O—H···O=C ⇌ O$^-$···H—O$^+$=C.

The intensity ratio of the bands corresponding to the groups involved in hydrogen bonding reveals pronounced transfer of protons due to the hydrogen bonding in considered species. However, these spectral features coexist together with those due to the intermoleculary hydrogen-bonded C=O group, similar to that for chloranilic acid. This indicates that proton transfer is not carried out throughout the crystals but occurs rather in a discontinuous manner.

EXPERIMENTAL SECTION

Preparation. Chloranilic acid dihydrate was freshly prepared by the method of Gräbe.[114] Anhydrous acid was obtained by drying the dihydrate over silica gel as described by Andersen;[95] single crystals were obtained by recrystallization from anhydrous ethanol in a dry atmosphere.

The samples studied were prepared and crystallized in a dry environment from anhydrous ethanol by evaporation for 2−3 months. Even a small amount of water results in the formation of hydrates.[93] In order to obtain data on hydrogen bonding of comparable accuracy, the crystal structure of anhydrous chloranilic acid was redetermined.

The samples prepared were rather inhomogenous and contained, besides the desired crystals, free chloranilic acid, alkali carbonate, potassium (or rubidium) chloranilate, and even traces of their hydrates (due to a small quantity of water produced by neutralization of the acid with carbonate).[99] The single crystals of the studied compounds were small and rather sensitive to moisture, X-rays, and temperature changes. Lowering or raising the temperature drastically increased mosaicity and degraded quality of the measured data. Therefore, only room-temperature measurement provided data accurate enough for location of the proton. 100 and 320 K data could be used for location of heavy atoms only.

X-ray Structure Analysis. Single crystal measurements at room temperature (293 K) and 100 K were performed on an Oxford Xcalibur Nova R diffractometer with a microfocus tube (Cu Kα radiation, CCD detector). The instrument is equipped with an Oxford Instruments CryoJet liquid-nitrogen cooling device. The CrysAlis PRO program package[115] was used for data reduction and multiscan absorption correction. Measurements above room temperature (320 and 340 K) were performed on an Enraf-Nonius CAD-4 diffractometer (Cu Kα radiation, point detector, three standard reflections measured every 120 min for intensity control) equipped with an Oxford Cryosystems Series 700 liquid-nitrogen cryostat. The standard WinGX routine was used for data reduction.[116] Only unit cell parameters were measured at 340 K. However, due to increased mosaicity and (at temperatures over 293 K) increased atomic motion, the data obtained were inferior to room-temperature measurements. Therefore, only positions of non-H atoms could be reliably determined.

The structures were solved with SHELXS97[117] and refined with SHELXL97.[117] The models were refined using the full-matrix least-squares refinement. Hydrogen atoms were located from difference Fourier maps and refined as free entities. The atomic scattering factors were those included in SHELXL97.[117] Molecular geometry calculations were performed with PLATON,[118] and molecular graphics were prepared using ORTEP-3[119] and CCDC-Mercury.[120] Crystallographic and refinement data for the structures reported are shown in Table 6.

The difference Fourier map in Figure 4 was calculated after the proton H was omitted from a completely refined structure.

Supplementary crystallographic data for this paper can be obtained free of charge via www.ccdc.cam.ac.uk/conts/retrieving.html (or from the Cambridge Crystallographic Data Centre, 12 Union Road, Cambridge CB2 1EZ, U.K.; fax: +44 1223 336033; or deposit@ccdc.cam.ac.uk). CCDC-805078-805082 contain the supplementary crystallographic data for this paper.

IR Spectroscopy. Infrared spectra were measured on an ABB Bomem MB102 FT-IR spectrometer with caesium iodide optics and a deuterated triglycylsulphate (DTGS) detector. The range of measurement was 4000−500 cm^{-1}, and the resolution was 4 cm^{-1}. The attenuated total reflection (ATR) technique was used. $Rb_2[CA(H_2CA)]$ and $K_2[CA(H_2CA)]$ are sensitive to moisture and high pressure and would also react with KBr, rendering the KBr pellet technique useless.

Solid State NMR. ^{1}H magic-angle spinning (MAS) NMR spectra were recorded on a 600 MHz Varian NMR system, operating at a ^{1}H Larmor frequency of 599.87 MHz, with a rotation synchronized Hahn-echo pulse sequence. The sample rotation frequency was 20 kHz, the repetition delay between consecutive scans was 80 s, and the number of scans was four. Chemical shifts of ^{1}H signals were referenced to the signal of tetramethylsilane.

Computational Methods. We used the plane-wave DFT approach, implemented in the CPMD v 3.13.2 program package.[121] Since potassium and rubidium chloranilate are reasonably similar in all crucial aspects considered in this study, we confined our computational treatment to the potassium salt. The electron density of the system was expressed in the plane-wave basis set with a kinetic energy cutoff of 80 Ry. The core electrons were approximated with atomic pseudopotentials of Troullier and Martins.[122] The BLYP density functional was used throughout. Fully featured periodic boundary conditions were employed, and the unit cell parameters and initial atomic positions were built up according to the crystallographic data collected at room temperature (Table 6).

The most relevant structural motifs for the study of proton transfer are the ...H_2CA···CA^{2-}... chains which are aligned with the long [111] unit cell diagonal. Therefore, we considered in addition to the simple unit cell also the [2 2 2; 0 1 0; 0 0 1] and

Table 6. Crystallographic, Data Collection and Refinement Details

compound	H_2CA	$Rb_2[CA(H_2CA)]$	$K_2[CA(H_2CA)]$ (293 K)
Brutto formula	$C_6Cl_2H_2O_4$	$C_{12}Cl_4H_2O_8Rb_2$	$C_{12}Cl_4H_2O_8K_2$
formula wt/g mol^{-1}	208.98	586.88	494.14
crystal dimensions/mm	0.26 × 0.24 × 0.12	0.25 × 0.08 × 0.05	0.15 × 0.05 × 0.03
space group	$P2_1/n$	$P\bar{1}$	$P\bar{1}$
a/Å	7.5755 (2)	3.980 (3)	3.8756 (3)
b/Å	5.5389 (1)	7.945 (3)	7.7935 (4)
c/Å	8.7046 (2)	13.38 (1)	13.2123 (9)
α/deg	90	100.44 (6)	99.497 (5)
β/deg	104.043 (2)	96.62 (6)	95.564 (5)
γ/deg	90	92.64 (4)	91.355 (5)
Z	2	1	1
V/Å^3	354.33 (1)	412.3 (5)	391.43 (5)
D_{calc}/g cm^{-3}	1.959	2.363	2.096
μ/mm^{-1}	8.036	14.081	12.077
T/K	293 (2)	293 (2)	293 (2)
Θ range/deg	6.96−75.92	3.39−76.53	3.41−76.05
range of h, k, l	$-9 > h > 9$;	$-5 > h > 4$;	$-4 > h > 4$
	$-6 > k > 6$;	$-9 > k > 9$;	$-9 > k > 9$;
	$-9 > l > 10$	$-16 > l > 16$	$-16 > l > 16$
reflections collected	1756	4327	3971
independent reflections	717	1664	1549
observed reflections ($I \geq 2\sigma$)	685	1526	1428
R_{int}	0.0160	0.0308	0.0331
$R(F)$	0.0338	0.0431	0.0476
$R_w(F^2)$	0.0965	0.1207	0.1333
goodness of fit	1.133	1.033	1.088
no. of parameters	59	122	122
$\Delta\rho_{max}$, $\Delta\rho_{min}$ (e Å^{-3})	0.271; −0.241	0.715; −0.739	0.683; −0.479

compound	$K_2[CA(H_2CA)]$ (100 K)	$K_2[CA(H_2CA)]$ (320 K)	$K_2[CA(H_2CA)]$ (340 K)
Brutto formula	$C_6Cl_2H_2O_4$	$C_{12}Cl_4H_2O_8K_2$	$C_{12}Cl_4H_2O_8K_2$
formula wt/g mol^{-1}	494.14	494.14	494.14
crystal dimensions/mm	0.20 × 0.05 × 0.04	0.18 × 0.07 × 0.06	0.18 × 0.07 × 0.06
space group	$P\bar{1}$	$P\bar{1}$	$P\bar{1}$
a/Å	3.8161 (3)	3.8849 (9)	3.971 (9)
b/Å	7.7755 (8)	7.773 (5)	7.764 (6)
c/Å	13.1292 (9)	13.235 (4)	13.438 (6)
α/deg	99.606 (7)	99.46 (4)	99.4 (1)
β/deg	94.968 (6)	95.77 (2)	95.4 (3)
γ/deg	91.248 (7)	91.30 (4)	91.4 (1)
Z	1	1	1
V/Å^3	382.40 (6)	391.9 (3)	396 (1)
D_{calc}/g cm^{-3}	2.146	2.093	
μ/mm^{-1}	12.362	12.061	
T/K	100 (2)	320 (2)	340 (2)
Θ range/deg	3.43−76.07	5.78−70.69	
range of h, k, l	$-4 > h > 4$;	$-4 > h > 4$;	
	$-9 > k > 9$;	$-9 > k > 0$;	
	$-16 > l > 16$	$-15 > l > 16$	
reflections collected	3306	1963	
independent reflections	1570	1507	
observed reflections ($I \geq 2\sigma$)	1520	1145	
R_{int}	0.0441	0.1141	
$R(F)$	0.0452	0.0900	

dx.doi.org/10.1021/jp112380f |J. Phys. Chem. A 2011, 115, 3154–3166

Table 6. Continued

compound	$K_2[CA(H_2CA)]$ (100 K)	$K_2[CA(H_2CA)]$ (320 K)	$K_2[CA(H_2CA)]$ (340 K)
$R_w(F^2)$	0.1242	0.2493	
goodness of fit	1.066	1.034	
no. of parameters	122	122	
$\Delta\rho_{max}$, $\Delta\rho_{min}$ (e Å^{-3})	0.719; −0.566	0.824; −2.039	

[3 3 3; 0 1 0; 0 0 1] supercells in order to increase the number of $H_2CA\cdots CA^{2-}$ pairs in the cell and thus reduce the correlation within the hydrogen-bonded chain. For each of the three models differing in the choice of the unit cell (referred to as the single, double, and triple cell model hereinafter), full and partial geometry optimizations were performed, keeping the unit cell parameters fixed. The optimization of structures containing solely $H_2CA\cdots CA^{2-}$ chains (no proton transfer) was performed using the symmetry constraints of the $P\bar{1}$ space group.

Additionally, we attempted to obtain fully optimized structures with one of the protons transferred over the hydrogen bond. This was done in two steps. In the first step, the proton was shifted nearer to the acceptor oxygen (O4) and the structure was partially optimized with the constraint of the H−O4 distance being fixed to 1.0 Å, ensuring the substantial changes of bond lengths in the vicinity of the hydrogen bond. In the second step, the constraint was removed and the structure was reoptimized to a regular minimum. As the $P\bar{1}$ symmetry is broken by displacing one proton (but not others), the simple $P1$ symmetry was used in these calculations.

We characterized the proton transfer process by performing a relaxed potential energy function scan. A selected proton was moved along the hydrogen bond in 0.1 Å steps, spanning the range of the O2−H distance between 0.8 and 1.8 Å. At each step, the structure was partially optimized with the constraint of the fixed O−H distance. The $P1$ symmetry was assumed in the calculations of proton potentials.

We performed a tentative molecular dynamics (MD) run on the triple cell model using the Car−Parrinello methodology[123] with a time step of 4 au (0.096752), a fictitious orbital mass of 500 electron masses, and a temperature of 300 K. The temperature was enforced to the specified value by using the Nosé−Hoover thermostat[124] with a coupling frequency of 1500 cm^{-1}. An initial step of ∼1 ps was taken as equilibration and discarded, while the production phase was about 2 ps long. Note that this MD run took over 3 weeks to complete, and we did not proceed with additional simulations due to CPU economy; the results of the MD simulation were used as a qualitative demonstration of the nature and time scale of the proton transfer dynamics.

NMR chemical shift calculations were carried out by utilizing the linear response methodology implemented in the CPMD program package.[125] All ^{1}H shifts were computed relative to the proton resonance signal of a free tetramethylsilane molecule modeled in an isolated cubic box of 16 Å. As the calculated shifts were found to vary with the unit cell size, sufficiently large supercells were used in order to get converged values. Interestingly, the variation was much larger when the angles of the unit cell notably deviated from 90° (e.g., double and triple cell described above) than in the conventional unit cell which is not far from being orthogonal. Additional motivation to use large supercells is in the fact that k-point sampling is not supported for linear response calculations. Thus, all structures considered for NMR calculations were mapped to the [2 2 2; 0 2 0; 0 0 2] or [3 3 3; 0 2 0; 0 0 2] supercell. Since point group symmetry is also not supported for this type of calculation, the chemical shift values of otherwise equivalent atoms were not exactly identical; hence, the result is given as their average; nevertheless, the deviations were relatively small (∼0.1 ppm).

All calculations were performed at the computer cluster of National Institute of Chemistry (PC/Linux workstations). Typically, calculations utilized from 8 to 64 processors at a time.

■ ASSOCIATED CONTENT

Supporting Information. Details on the geometry of molecules of chloranilic acid and its dianion at various temperatures as well as details on cation coordination. This material is available free of charge via the Internet at http://pubs.acs.org.

■ AUTHOR INFORMATION

Corresponding Author
*E-mail: kojic@irb.hr.

■ ACKNOWLEDGMENT

We thank the Ministry of Science, Education and Sport of the Republic of Croatia for financing (Grant Nos. 098-1191344-2943 and 098-0982904-2927) and bilateral scientific collaboration between Croatia and Slovenia. Financial support of the Slovenian Research Agency (Grant No. 1000-07-219779 and P1-0012) is also gratefully acknowledged. The authors thank Prof. Dušan Hadži (NIC) for valuable suggestions concerning measurement and interpretation of IR and solid-state NMR spectra and Dr. Jelena Veljković (RBI) for participating in discussion on a solution NMR spectrum.

■ REFERENCES

(1) Huggins, M. L. Undergraduate Thesis, University of California, 1919.
(2) Latimer, W. M.; Rodebush, W. H. *J. Am. Chem. Soc.* **1920**, *42*, 1419–1433.
(3) Kojić-Prodić, B.; Molčanov, K. *Acta Chim. Slov.* **2008**, *55*, 692–708.
(4) Pauling, L. *The Nature of the Chemical Bond*; Cornell University Press: Ithaca, NY, 1939.
(5) Pimentel, G. C.; McClellan, A. L. *The Hydrogen Bond*; Freeman: San Francisco, CA, 1960.
(6) Hadži, D., Ed. *Theoretical Treatments of Hydrogen Bonding*; Wiley: Stuttgart, Germany, 1997.
(7) Jeffrey, G. A. *An Introduction to Hydrogen Bonding*; Oxford University Press: Oxford, U.K., 1997.
(8) Scheiner, S. *Hydrogen Bonding*; Oxford University Press: Oxford, U.K., 1997.
(9) Steiner, T. *Angew. Chem., Int. Ed.* **2002**, *41*, 41–76.
(10) Schowen, R. L., Ed. *Handbook of Hydrogen Transfer*; Wiley-VCH: Stuttgart, Germany, 2006.

(11) Hynes, J. T.; Klinman, J. P.; Limbach, H.-H.; Schowen, R. L. *Hydrogen-Transfer Reactions*; Wiley-VCH: Stuttgart, Germany, 2007.
(12) Tuckerman, M. E.; Marx, D.; Klein, M. L.; Parrinello, M. *Science* **1997**, *275*, 817–820.
(13) Marx, D.; Tuckerman, M. E.; Hutter, J.; Parrinello, M. *Nature (London)* **1999**, *397*, 601–604.
(14) Ludwig, R. *ChemPhysChem* **2004**, *5*, 1495–1497.
(15) Lapid, H.; Agmon, N.; Peterson, M. K.; Voth, G. A. *J. Chem. Phys.* **2005**, *122*, o14506.
(16) Markovitch, O.; Agmon, N. *J. Phys. Chem. A* **2007**, *111*, 2253–2256.
(17) Agmon, N. *Chem. Phys. Lett.* **2000**, *319*, 247–252.
(18) Olovsson, I. *Z. Phys. Chem.* **2006**, *220*, 963–978.
(19) Perrin, C. L.; Nielson, J. B. *Annu. Rev. Phys. Chem.* **1997**, *48*, 511–544.
(20) Isaacs, E. D.; Shukla, A.; Platzman, P. M.; Hamann, D. R.; Barbiellini, B.; Tulk, C. A. *Phys. Rev. Lett.* **1999**, *82*, 600–603.
(21) Elsaesser, T.; Bakker, H. J. *Ultrafast Hydrogen Bonding Dynamics and Proton Transfer Processes in the Condensed Phase*; Kluwer: Dordrecht, The Netherlands, 2002.
(22) Marx, D. *ChemPhysChem* **2006**, *7*, 1848–1870.
(23) Peters, K. S. *Acc. Chem. Res.* **2009**, *42*, 89–96.
(24) Roscioli, J. R.; McCunn, L. R.; Johnson, M. A. *Science* **2007**, *316*, 249–1254.
(25) Swanson, J. M. J.; Simmons, J. *J. Phys. Chem. B* **2009**, *113*, 5149–5161.
(26) Ludwig, R. *ChemPhysChem* **2007**, *8*, 44–46.
(27) Tuckerman, M. E.; Marx, D.; Parrinello, M. *Nature (London)* **2002**, *417*, 925–929.
(28) Asthagiri, D.; Pratt, L. R.; Kress, J. D.; Gomes, M. A. *Proc. Natl. Acad. Sci. U.S.A.* **2004**, *101*, 7229–7233.
(29) Zheng, Sun; Chi-Kit, Siu; Petru Balaj, O.; Gruber, M.; Bondybey, V. E.; Beyer, M. K. *Angew. Chem., Int. Ed.* **2006**, *45*, 4027–4030.
(30) Kirchner, B. *ChemPhysChem* **2007**, *8*, 41–43.
(31) Kaledin, M.; Kaledin, A. L.; Bowman, J. M. *J. Phys. Chem. A* **2006**, *110*, 2933–2939.
(32) Gale, J. D. *Solid State Sci.* **2006**, *8*, 234–240.
(33) Pirc, G.; Stare, J.; Mavri, J. *J. Chem. Phys.* **2010**, *132*, 224506–224512.
(34) Horiuchi, S.; Tokunaga, Y.; Giovannetti, G.; Picozzi, S.; Itoh, H.; Shimano, R.; Kumai, R.; Tokura, Y. *Nature* **2010**, *463*, 789–793.
(35) Horsewill, A. J.; McGloin, C. J.; Trommsdorff, H. P.; Johnson, M. R. *Chem. Phys.* **2003**, *391*, 41–52.
(36) Wilson, C. C.; Goeta, A. E. *Angew. Chem., Int. Ed.* **2004**, *43*, 2095–2099.
(37) Parkin, A.; Harte, S. M.; Goeta, A. E.; Wilson, C. C. *New J. Chem.* **2004**, *28*, 718–721.
(38) Wilson, C. C.; Morrison, C. A. *Chem. Phys. Lett.* **2002**, *395*, 85–89.
(39) Parkin, A.; Adam, M.; Cooper, R. I.; Middlemiss, D. S.; Wilson, C. C. *Acta Crystallogr., Sect. B* **2007**, *B63*, 303–308.
(40) Martins, D. M .S.; Middlemiss, D. S.; Pulham, C. R.; Wilson, C. C.; Weller, M. T.; Henry, P. F.; Shankland, N.; Shankland, K.; Marshall, W. G.; Ibbeerson, R. M.; Knight, K.; Moggach, S.; Brunelli, M.; Morrison, C. A. *J. Am. Chem. Soc.* **2009**, *131*, 3884–3893.
(41) Morrison, C. A.; Siddick, M. M.; Camp, P. J.; Wilson, C. C. *J. Am. Chem. Soc.* **2005**, *127*, 4042–4048.
(42) Nygren, C. A.; Wilson, C. C.; Turner, J. F. C. *J. Phys. Chem. A* **2005**, *109*, 1911–1919.
(43) Wilson, C. C. *Acta Crystallogr., Sect. B* **2001**, *B57*, 435–439.
(44) Steiner, T.; Majerz, I.; Wilson, C. C. *Angew. Chem., Int. Ed.* **2001**, *40*, 2561–2564.
(45) Vishweshwar, P; Babu, N. J.; Nangia, A.; Mason, S. A.; Puschmann, H.; Mondal, R.; Howard, J. A. K. *J. Phys. Chem. A* **2004**, *108*, 9406–9416.
(46) Cowan, J. A.; Howard, J. A. K.; McIntyre, G. J.; Lo, S. M.-F.; Williams, I. D. *Acta Crystallogr., Sect. B* **2005**, *B61*, 724–730.
(47) Wilson, C. C.; Thomas, L. H. *C. R. Chim.* **2005**, *8*, 1434–1443.
(48) Wilson, C. C.; Xu, X.; Florence, A. J.; Shankland, N. *New J. Chem.* **2006**, *30*, 979–981.
(49) Szafranski, M.; Katrusiak, A.; McIntyre, G. J. *Cryst. Growth Des.* **2010**, *10*, 4334–4338.
(50) Katrusiak, A. Hydrogen-bonded Crystals of Exceptional Dielectric Properties. In *Engineering of Crystalline Materials Properties: State of the Art in Modelling, Design and Applications*; Novoa, J. J., Braga, D., Addadi, L., Eds.; Springer: Dordrecht, The Netherlands, 2008; pp 231−250.
(51) Zundel, G.; Metzger, H. *Z. Phys. Chem.* **1968**, *58*, 225–245.
(52) Zundel, G.; Fritsch, J. *J. Phys. Chem.* **1984**, *88*, 6295–6302.
(53) Lindemann, R.; Zundel, G. *J. Chem. Soc., Faraday Trans. 2* **1977**, *73*, 788–803.
(54) Janoschek, R.; Weidemann, E. G.; Pfeiffer, H.; Zundel, G. *J. Am. Chem. Soc.* **1972**, *94*, 2387–2396.
(55) Weidemann, E. G.; Zundel, G. *Z. Naturforsch., A* **1970**, *25*, 627–634.
(56) Schloeberg, D.; Zundel, G. *J. Chem. Soc., Faraday Trans 2* **1973**, *69*, 771.
(57) Kramer, R.; Zundel, G.; Brzezinski, B.; Olejnik, J. *Faraday Trans.* **1992**, *88*, 1659.
(58) Langner, R.; Zundel, G. *Faraday Trans.* **1995**, *91*, 3831.
(59) Fontaine-Vive, F.; Johnson, M. R.; Kearley, G. J.; Howard, J. A. K.; Parker, S. F. *J. Am. Chem. Soc.* **2006**, *128*, 2963–2969.
(60) Piccoli, P. M. B.; Koetzle, T. F.; Schultz, A. J.; Zhurova, E. A.; Stare, J.; Pinkerton, A. A.; Eckert, J.; Hadži, D. *J. Phys. Chem. A* **2008**, *112*, 6667–6677.
(61) Gajda, R.; Katrusiak, A. *Acta Crystallogr., Sect. B* **2007**, *B63*, 896–902.
(62) Olejniczak, A.; Katrusiak, A. *CrystEngComm* **2010**, *12*, 2528–2532.
(63) Katrusiak, A. *Acta Crystallogr., Sect. B* **2008**, *B64*, 135–148.
(64) Braun-Sand, S.; Olsson, M. H. M.; Mavri, J. Computer Simulations of Proton Transfer in Proteins and Solutions in Hydrogen-Transfer Reactions. In *Hydrogen-Transfer Reactions*; Hynes, J. T., Klinman, J. P., Limbach, H.-H., Schowen, R. L., Eds.; Wiley-VCH: Stuttgart, Germany, 2007.
(65) Garcia-Viloca, M.; Gao, J.; Karplus, M.; Truhlar, D. G. *Science* **2004**, *303*, 186–195.
(66) Warshel, A. *Annu. Rev. Biophys. Biomol. Struct.* **2003**, *32*, 425–443.
(67) Cleland, W. *Biochemistry* **1992**, *31*, 317–319.
(68) Cleland, W. W.; Kreevoy, M. M. *Science* **1994**, *264*, 1887–1890.
(69) Frey, P. A.; Whitt, S. A.; Tobin, J. B. *Science* **1994**, *264*, 1927–1930.
(70) Frey, P. A. *Science* **1995**, *268*, 189.
(71) Cleland, W. W.; Frey, P. A.; Gerlt, J. A. *J. Biol. Chem.* **1998**, *273*, 25529–25532.
(72) Cleland, W. W. *Arch. Biochem. Biophys.* **2000**, *382*, 1–5.
(73) Frey, P. A. *Magn. Reson. Chem.* **2001**, *39*, S190–S198.
(74) Kuhn, P.; Knapp, M.; Soltis, S. M.; Ganshaw, G.; Thoene, M.; Bott, R. *Biochemistry* **1998**, *37*, 13446–13452.
(75) Bachovchin, W. W. *Magn. Reson. Chem.* **2001**, *39*, S199–S213.
(76) Ash, E. L.; Sudmeier, J. L.; De Fabo, E. C.; Bachovchin, W. W. *Science* **1997**, *278*, 1128–1132.
(77) Schutz, C. N.; Warshel, A. *Proteins: Struct., Funct., Bioinf.* **2004**, *55*, 711–723.
(78) Shokhen, M.; Albeck, A. *Proteins: Struct., Funct., Bioinf.* **2004**, *54*, 468–477.
(79) Tamada, T.; Kinoshita, T.; Kurihara, K.; Adachi, M.; Ohhara, T.; Imai, K.; Kuroki, R.; Tada, T. *J. Am. Chem. Soc.* **2009**, *131*, 11033–11040.
(80) Mullholand, A. J. *Chem. Cent. J.* **2007**, *1*, 1–19.
(81) Claeyssens, F.; Harvey, J. N.; Manby, F. R.; Mata, R. A.; Mullholand, A. J.; Ranaghan, K. E.; Schütz, M.; Thiel, S.; Thiel, W.; Werner, H. J. *Angew. Chem., Int. Ed.* **2006**, *45*, 6856–6859.
(82) Meyer, M. P.; Tomchick, D. R.; Klinman, J. P. *Proc. Natl. Acad. Sci. U.S.A.* **2008**, *105*, 1146–1151.
(83) Olsson, M.; Sieghban, P. E. M.; Warshel, A. *J. Am. Chem. Soc.* **2004**, *126*, 2820–2828.
(84) Kamerlin, S. C. L.; Mavri, J.; Warshel, A. *FEBS Lett.* **2010**, *584*, 2759–2766.

(85) Molčanov, K.; Kojić-Prodić, B.; Roboz, M. *Acta Crystallogr, Sect. B* **2006**, *B62*, 1051–1060.
(86) Kawata, S.; Kitagawa, S. *Coord. Chem. Rev.* **2002**, *224*, 11–34.
(87) Noro, S.; Kitagawa, S.; Kitaura, R. *Angew. Chem., Int. Ed.* **2004**, *43*, 2334–2375.
(88) Matsuda, R.; Kitagawa, S. *Coord. Chem. Rev.* **2007**, *251*, 2490–2509.
(89) Tokura, Y.; Horiuchi, S.; Kumai, R. *Chem. Commun.* **2007**, 2321–2329.
(90) Okumoto, Y.; Kumai, R.; Horiuchi, S. *J. Chem. Phys.* **2006**, *125*, 084715.
(91) Di Pasquale, A. G.; Miller, J. S.; Min, K. S.; Rheingold, A. L. *Inorg. Chem.* **2006**, *45*, 6135–6137.
(92) Golen, J. A.; Rheingold, A. L.; Miller, J. S.; Min, K. S.; DiPasquale, A. G. *J. Am. Chem. Soc.* **2007**, *129*, 2360–2368.
(93) Molčanov, K.; Kojić-Prodić, B.; Meden, A. *CrystEngComm* **2009**, *11*, 1407–1415.
(94) Molčanov, K.; Kojić-Prodić, B. *CrystEngComm* **2010**, *12*, 925–939.
(95) Andersen, E. K. *Acta Crystallogr.* **1967**, *22*, 188–191.
(96) Matsuda, H.; Osaki, K.; Nitta, I. *Bull. Chem. Soc. Jpn.* **1958**, *31*, 611–620.
(97) Sakurai, T. *Acta Crystallogr.* **1965**, *19*, 320–330.
(98) Sakurai, T. *Acta Crystallogr, Sect. B* **1968**, *24*, 403–412.
(99) Molčanov, K.; Kojić-Prodić, B.; Meden, A. *Croat. Chem. Acta* **2009**, *82*, 387–396.
(100) Kashino, S.; Ishida, H. *Z. Naturforsch., A* **2002**, *57*, 829–836.
(101) Szabó, A.; Kovács, A. *J. Mol. Struct.* **1999**, *510*, 215–225.
(102) Pawlukojć, A.; Bator, G.; Sobczyk, L.; Grech, E.; Nowicka-Scheibe, J. *J. Phys. Org. Chem.* **2003**, *16*, 709–714.
(103) Hattori, K.; Ishiuchi, S.; Fujii, M.; Howard, D. L; Kjaergaard, H. G. *J. Phys. Chem. A* **2007**, *111*, 6028–6033.
(104) Nyquist, R. A.; Luoma, D. A.; Putzig, C. L. *Vib. Spectrosc.* **1992**, *3*, 181–210.
(105) Mikenda, W.; Steinböck, S. *J. Mol. Struct.* **1996**, *384*, 159–163.
(106) Park, M.; Shin, I.; Singh, N. J.; Kim, K. S. *J. Phys. Chem. A* **2007**, *111*, 10692–10702.
(107) Asmis, K. R.; Pivonka, N. L.; Santamborgio, G.; Brümmer, M.; Kaposta, C.; Neumark, D. M.; Wöste, L. *Science* **2003**, *299*, 1375–1377.
(108) Rousseau, R.; Kleinschmidt, V.; Schmidt, U. W.; Marx, D. *Angew. Chem., Int. Ed.* **2004**, *43*, 4804–4807.
(109) Munshi, P.; Madsen, A. Ø.; Spackman, M. A.; Larsen, S.; Destro, R. *Acta Crystallogr, Sect. A* **2008**, *A64*, 46–475.
(110) Müller, P., Ed. *Crystal Structure Refinement-A Crystallographer's Guide to SHELXL*; Oxford University Press: Oxford, U.K., 2006.
(111) Mikenda, W. *J. Mol. Struct.* **1986**, *147*, 1–15.
(112) Stare, J.; Jezierska, A.; Ambrožič, G.; Košir, I. J.; Kidrič, J.; Koll, A.; Mavri, J.; Hadži, D. *J. Am. Chem. Soc.* **2006**, *126*, 4437–4443.
(113) Garcia-Viloca, M.; Gelabert, R.; Gonzales-Lafont, A.; Moreno, M.; Lluch, J. M. *J. Am. Chem. Soc.* **1998**, *120*, 10203–10209.
(114) Vanino, L., Ed. *Handbuch der syntetischen Chemie*; F. Enke Verlag: Stuttgart, Germany, 1937.
(115) *CrysAlis PRO*; Oxford Diffraction Ltd.: Oxford, U.K.
(116) Harms, K.; Wocadlo, S. *XCAD-4. Program for Processing CAD-4 Diffractometer Data*; University of Marburg: Marburg, Germany, 1995.
(117) Sheldrick, G. M. *Acta Crystallogr, Sect. A* **2008**, *A64*, 112–122.
(118) Spek, A. L. *J. Appl. Crystallogr.* **2003**, *36*, 7–13.
(119) Faruggia, L. J. *J. Appl. Crystallogr.* **1997**, *30*, 565.
(120) McCabe, P.; Pidcock, E.; Shields, G. P.; Taylor, R.; Towler, M.; Macrae, C. F.; Edgington, P. R.; van de Streek, J. *J. Appl. Crystallogr.* **2006**, *39*, 453–457.
(121) Boero, M.; Curioni, A.; Hutter, J.; Isayev, A.; Kohlmeyer, A.; Nair, N.; Quester, W.; Walewski, Ł. *Car-Parrinello Molecular Dynamics*; 1990−2008.
(122) Troullier, N.; Martins, J. L. *Phys. Rev. B* **1991**, *43*, 1993–2006.
(123) Car, R.; Parrinello, M. *Phys. Rev. Lett.* **1985**, *55*, 2471–2474.
(124) Nosé, S. *J. Chem. Phys.* **1984**, *81*, 511–519.
(125) Sebastiani, D.; Parrinello, M. *J. Phys. Chem. A* **2001**, *105*, 1951–1958.